AIP Review of Scientific Instruments

Development of a compact, fiber-coupled, six degree-of-freedom measurement system for precision linear stage metrology

Xiangzhi Yu, Steven R. Gillmer, Shane C. Woody, and Jonathan D. Ellis

Citation: Review of Scientific Instruments **87**, 065109 (2016); doi: 10.1063/1.4953335
View online: http://dx.doi.org/10.1063/1.4953335
View Table of Contents: http://scitation.aip.org/content/aip/journal/rsi/87/6?ver=pdfcov
Published by the AIP Publishing

REVIEW OF SCIENTIFIC INSTRUMENTS **87**, 065109 (2016)

Development of a compact, fiber-coupled, six degree-of-freedom measurement system for precision linear stage metrology

Xiangzhi Yu,[1,a)] Steven R. Gillmer,[1] Shane C. Woody,[2] and Jonathan D. Ellis[1,3]
[1]*Department of Mechanical Engineering, University of Rochester, Rochester, New York 14627, USA*
[2]*InSituTec Incorporated, 7140 Weddington Road, Concord, North Carolina 28027, USA*
[3]*The Institute of Optics, University of Rochester, Rochester, New York 14627, USA*

(Received 4 February 2016; accepted 23 May 2016; published online 13 June 2016)

A compact, fiber-coupled, six degree-of-freedom measurement system which enables fast, accurate calibration, and error mapping of precision linear stages is presented. The novel design has the advantages of simplicity, compactness, and relatively low cost. This proposed sensor can simultaneously measure displacement, two straightness errors, and changes in pitch, yaw, and roll using a single optical beam traveling between the measurement system and a small target. The optical configuration of the system and the working principle for all degrees-of-freedom are presented along with the influence and compensation of crosstalk motions in roll and straightness measurements. Several comparison experiments are conducted to investigate the feasibility and performance of the proposed system in each degree-of-freedom independently. Comparison experiments to a commercial interferometer demonstrate error standard deviations of 0.33 μm in straightness, 0.14 μrad in pitch, 0.44 μrad in yaw, and 45.8 μrad in roll. *Published by AIP Publishing.* [http://dx.doi.org/10.1063/1.4953335]

I. INTRODUCTION

There is an increasing need for higher accuracy and resolution in ultraprecision manufacturing and inspection systems including lithography stages, biological scanning instruments, and nanofabrication positioning equipment. Most of these precision systems employ a series of stacked linear stages to provide accurate multiple degree-of-freedom (DOF) positioning of a probe, tool, or sample. The systems must be calibrated during subassembly to attain error mapping and require routine calibrations to verify that process equipment meets specific inspection and manufacturing specifications. There are six geometric motion errors associated with a precision linear stage. The main movement along the z-axis is the displacement, Δz; there are two parasitic lateral errors (straightness errors), Δx and Δy, and three rotational errors, θ_x (pitch), θ_y (yaw), and θ_z (roll).

Optical interferometry is the preferred method of linear stage calibration due to its high dynamic range, high signal-to-noise ratio, and direct traceability to length standards.[1,2] Commercial interferometers typically use multiple configurations to provide accurate measurements for each DOF separately. As a result, a large body of work has been devoted to further improve the resolution and accuracy for displacement,[3–6] pitch and yaw,[7–10] straightness,[11–14] and roll.[15–17] In the referenced cases, the full calibration process may take multiple days since several setups and components are needed for multiple DOF measurements. Furthermore, extra calibration errors might be generated from these three areas: (1) temporal effects, where the increased time to calibrate exacerbates thermal drift; (2) dynamic errors, where the different sensor types have different masses causing a different dynamic behavior; and (3) location errors, where the sensor target must be placed at a specific location that does not coincide with the measurement point of interest.

To solve these problems, many metrology systems have been proposed to realize simultaneous measurement of all six degrees-of-freedom. Liu *et al.* used a commercial fiber-coupled laser interferometer and three parallel collimated laser beams to simultaneously measure six-DOF errors.[18] Li *et al.* developed a surface encoder for a planar motion stage by combining a three-axis angle sensor based on laser autocollimation with the three-axis displacement sensor based on a planar scale grating.[19] Qibo *et al.* developed a simple system for simultaneously measuring six-DOF geometric motion errors of a linear guide with compensation for laser beam drift errors.[20] Hsieh and Pan developed a grating-based interferometer composed of three identical detection parts utilizing heterodyne, grating shearing, and Michelson interferometry.[21] Chen *et al.* developed a laser straightness interferometer system with rotational error compensation to simultaneously measure six-DOF error parameters.[22] Even though these systems have the ability to measure all six DOFs simultaneously, the complex configurations, limited resolution, bulky size, need for custom optics, high cost, and large and heavy measurement targets are the significant shortcomings.

This study demonstrates a compact, fiber-coupled, six degree-of-freedom optical metrology system to provide fast, precise calibrations for linear stages using commercial off-the-shelf components. The novel design has the advantages of simplicity, compactness, and relatively low cost. Furthermore, the presented system minimally impacts the measured system's dynamic performance because it uses a single beam and a small measurement target (overall dimension and mass: 25 mm × 25 mm × 25 mm ≈ 50 g). In Secs. II–IV, the working principle for each DOF measurement is described in detail followed by experimental results and compensation methods for roll and straightness parasitic motions.

a)Electronic mail: xiangzhi.yu@rochester.edu.

II. WORKING PRINCIPLE

The schematic of the proposed 6-DOF interferometer is shown in Figure 1. Light from a stabilized laser source is split equally and directed towards two acoustic-optic modulators (AOMs), which are driven at slightly different RF frequencies to create a frequency difference between the two beams. After the AOMs, the first orders of the two beams are coupled into separate polarization maintaining fibers and then collimated back into free space. The f_1 beam passes through the top non-polarizing beam splitter (BS), reflects from the fixed reference mirror, and interferes with the f_2 beam that is reflected from the bottom BS at reference detector PD_R. Likewise, the f_2 beam passes through the bottom BS; half of the beam reflects from the retroreflector with a semi-reflective mirror (SRM) surface and interferes back at the bottom BS with the f_1 beam that is reflected from the top BS at the measurement quadrant photodetector (QPD). Meanwhile, the rest of the f_2 beam transmits through the semi-reflective coating, reflects through the retroreflector, and then transmits through the half-wave plate (HWP) which is fixed to the retroreflector to encode roll information. Afterwards, part of the beam is incident on the position sensitive detector (PSD) at nominally 13% of its original intensity due to beamsplitting. The remaining portion of the f_2 beam converges with the f_1 beam again to create an additional interference signal. In the end, the interference beam is equally split with half incident on reference detector PD_1 and the other incident on the roll measurement detector PD_2 through a polarizer. The relative intensities at PD_1 and PD_2 are approximately 7% of the original f_2 beam power interfering with 25% of the original f_1 beam power.

In Figure 1, the only stage-mounted component is the RR/SRM/HWP artifact—all other elements are fixed. Our SRM is a plate 50/50 non-polarizing beam splitter. For all experimental results presented in this publication, we have used modular components in a benchtop setup.

A. Displacement, pitch, and yaw

Part 1 adopts a differential wavefront sensing (DWS) technique which is used in The New Gravitational wave Observatory (NGO—formerly the Laser Interferometer Space Antenna—LISA) project to detect and accurately measure gravitational waves.[23–25] It utilizes a quadrant photodetector as the measurement detector to realize simultaneous measurements of displacement (Δz), pitch (θ_x), and yaw (θ_y). The individual phase change at each quadrant (A, B, C, and D) relative to the reference photodetector is detected and computed from the interference wavefront. The phase shift will be the same for all four quadrants if only a pure translation occurs. Thus, the overall displacement is determined by averaging the measured phase among all quadrants. However, the phase shift is different from quadrant to quadrant if there is an angular change between the two wavefronts, as indicated in Figure 2. Thus, pitch and yaw are determined by creating a weighted phase average over symmetrically adjacent quadrant detector pairs. The three DOFs are decoupled from DWS signals using

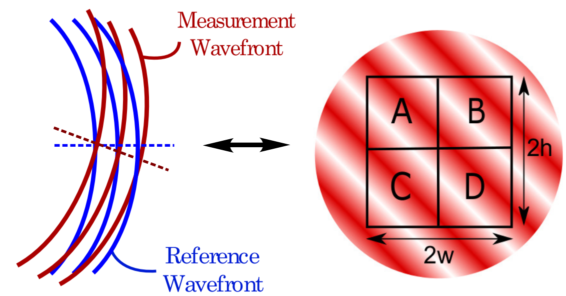

FIG. 2. Schematic of a quadrant photodetector for differential wavefront sensing with a tilted measurement wavefront. The quadrants are labeled A through D.

$$\Delta z \propto \frac{\phi_A + \phi_B + \phi_C + \phi_D}{4}, \tag{1}$$

$$\theta_x \propto \frac{(\phi_A + \phi_B) - (\phi_C + \phi_D)}{L_{pitch}}, \text{ and} \tag{2}$$

$$\theta_y \propto \frac{(\phi_A + \phi_C) - (\phi_B + \phi_D)}{L_{yaw}}, \tag{3}$$

where ϕ represents detected phase of quadrant A, B, C, or D, L_{pitch} and L_{yaw} represent a calibrated equivalent length in pitch and yaw measurements that is primarily dependent on beam diameter, detector size, alignment errors, and beam wavefront.

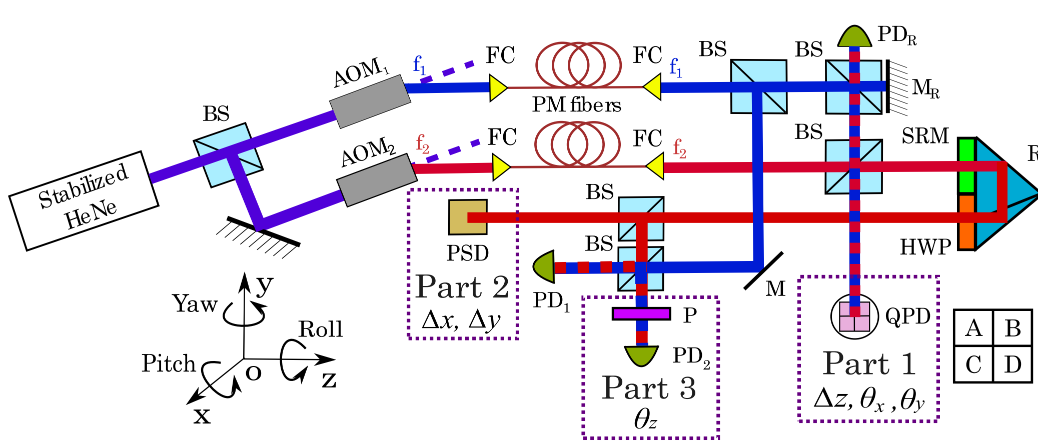

FIG. 1. Schematic of the six DOF interferometer (BS: beam splitter, AOM: acousto-optic modulator, FC: fiber coupler, PD: photodetector, M: mirror, SRM: semi-reflective mirror, HWP: half-wave plate, RR: retroreflector, QPD: quadrant photodetector, P: polarizer, and PSD: position sensitive detector).

A detailed description for this three DOF interferometer[26] and a model which effectively predicts the equivalent lengths (L_{pitch} and L_{yaw}) with high accuracy[27] are shown in our previous work.

B. Straightness

Part 2 utilizes a position sensitive detector (PSD) to determine the straightness (Δx and Δy) in two directions. The voltage readout of the PSD contains the centroid position information of the incident beam. The PSD has two normalized power outputs from −10 to 10 V that correspond to the beam center position from −10 to 10 mm across the entire PSD surface. Thus, the straightness errors can be determined by measuring the beam centroid change Δx_{PSD} and Δy_{PSD} on the PSD as

$$\Delta x = \frac{\Delta x_{PSD}}{2}, \tag{4}$$

$$\Delta y = \frac{\Delta y_{PSD}}{2}. \tag{5}$$

In practice, the coefficient will not exactly be 1/2, and a calibration factor is needed to achieve better accuracy. The straightness measurement based on the PSD method is simple and straightforward. The potential sensitivity and stability are primarily dependent on the PSD resolution and subsequent processing circuit which vary between manufacturers.

C. Roll

Part 3 uses the intensity change of an interference signal to determine the roll (θ_z) change. The final linear polarizer's axis is aligned with the horizontally polarized f_1 and f_2 beams, and the fast axis angle of HWP is γ with respect to the horizontal axis. The Jones matrices for all the elements in our roll measurement are represented by

$$E_1 = \begin{pmatrix} 1 \\ 0 \end{pmatrix}, \tag{6}$$

$$E_2 = \begin{pmatrix} 1 \\ 0 \end{pmatrix}, \tag{7}$$

$$H(\gamma) = \begin{pmatrix} \cos 2\gamma & \sin 2\gamma \\ \sin 2\gamma & -\cos 2\gamma \end{pmatrix}, \tag{8}$$

$$P = \begin{pmatrix} 1 & 0 \\ 0 & 0 \end{pmatrix}, \tag{9}$$

where E_1 and E_2 define the normalized amplitudes of the horizontally polarized f_1 and f_2 beams, $H(\gamma)$ is the HWP that is oriented at the angle γ with respect to the horizontal axis, and P represents the linear polarizer with axis of transmission horizontal. The final net electric field on the roll measurement detector PD_2 is

$$E = P[E_1 + H(\gamma)E_2]. \tag{10}$$

And the measured irradiance is calculated as

$$I = E^* E. \tag{11}$$

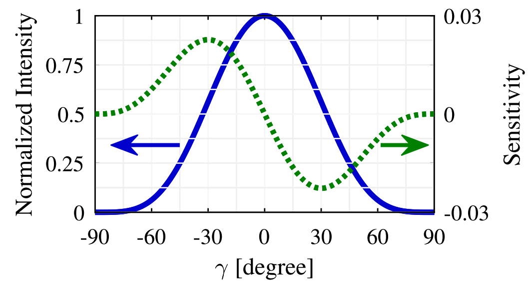

FIG. 3. Normalized intensity and sensitivity of the roll measurement signal with the HWP fast axis oriented from −90° to 90° with respect to the horizontal axis.

Figure 3 shows the simulation of the normalized intensity change and its sensitivity with the HWP fast axis angle rotated from −90° to 90° with respect to the horizontal axis. The plot indicates that the highest sensitivity occurs when the fast axis of the HWP is aligned at 30° or −30°, which is the initial condition for roll measurement in our system. When the measurement target has a small roll change which causes the fast axis of the HWP to rotate an angle around 30°, the normalized intensity change will be proportional to a roll (θ_z) change in a small linear region. The roll change can be calculated as

$$\theta_z = k\Delta I, \tag{12}$$

where k is the roll sensitivity and ΔI is the normalized intensity change of PD_2 which we measure using the amplitude readout from a lock-in amplifier (LIA). To perform the roll measurement with the LIA, the signals from PD_1 and PD_2 are sent to the reference and measurement channels, respectively. In practice, the coefficient k can be calibrated to achieve higher accuracy.

III. EXPERIMENTAL RESULTS

To experimentally investigate the performance and validate the working principle of the proposed system, we compare the measurement results of our six DOF system with a commercial interferometer (Renishaw XL-80) for each DOF movement separately on a five-axis nano-positioning stage (NewFocus five-axis positioner 8081), as shown in Figure 4. The five-axis stage is an open-loop system which can move along the X- and Z-axes and rotate about the X-, Y-, and Z-axes. Thus, we can record the comparison experiments for displacement, Δz; one straightness error, Δx; and three rotational errors, θ_x (pitch), θ_y (yaw), and θ_z (roll).

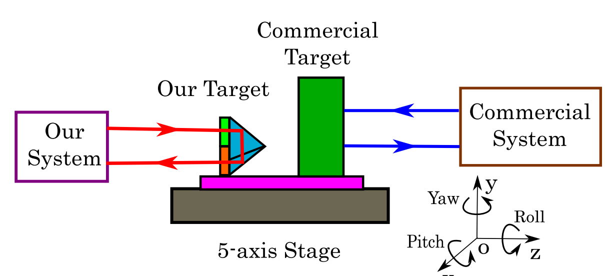

FIG. 4. Experimental setup comparing our six DOF system measurement results with a commercial interferometer for each DOF movement separately on a five-axis nano-positioning stage.

Our system uses a compact measurement target (overall dimension and mass: 25 mm × 25 mm × 25 mm ≈ 50 g) that contains a semi-reflective mirror, retro-reflector, and HWP, which gives all six DOF measurement results simultaneously. The target was constructed using a hollow retroreflector with a 50/50 non-polarizing plate beam splitter and HWP rigidly epoxied to input and output beam ports, respectively. The commercial measurement system utilizes various components and accessories to measure different DOFs and, most importantly, can only measure one DOF at a time. Thus, we keep our system the same but change the commercial system components and accessories in different DOF comparison experiments.

In the displacement comparison experiment, the nano-positioning stage moves back and forth along the Z-axis about 12 μm within 8 s and the two systems are measuring the same movement at opposite sides. The individual phase change in each quadrant A, B, C, and D relative to reference photodetector PD_R is measured by an FPGA-based phasemeter and post-processed by Eq. (1). As shown in Figure 5, the two measurement results agree with each other except during stage accelerations. Even though the two systems ideally measure the same movement, the targets' mass and residual compliances at their mounting points are different, which results in the discrepancy shown in the enlarged view. The effect is amplified when the stage suddenly moves. The majority of the 25.5 nm standard deviation is contributed to those two transient sections; however, we have previously demonstrated that this schematic can achieve sub-nanometer levels of accuracy and resolution for displacement.[26,27] Since the motion of the moving target introduces a Doppler shift to the measurement signal, the theoretical maximum measurement speed should satisfy $|v_m| < f_s\lambda/2$, where v_m is the maximum moving stage velocity, f_s is the split frequency in our system, and λ is the wavelength of the laser source. The current heterodyne frequency in our measurement system is set to 70 kHz which corresponds to a 0.022 m/s maximum stage velocity. For increased performance, AOMs that provide 1 MHz and 5 MHz split frequencies (corresponding to 0.32 m/s and 1.58 m/s maximum displacement speeds) can be incorporated. The measurement range for this type of heterodyne displacement interferometer is on the order of meters.

In the pitch comparison experiment, the nano-positioning stage rotates back and forth around the X-axis through a range of approximately 30 μrad within 8 s. The signal acquisition method remains the same as outlined above and pitch results can be calculated by Eq. (2) with the calibrated equivalent length for pitch, L_{pitch} = 1.8643 mm. For this result, the comparison system changes to a Renishaw angular interferometer with a large differential retro-reflector target. Figure 6 shows the pitch measurement comparison result and the standard deviation of the discrepancy is 0.12 μrad. Again, unequal target compliances affect the measurement during accelerations where vibrations occur, as shown in the enlarged view. The yaw comparison experiment is similar to pitch in which the stage rotates back and forth around the Y-axis through a range of 100 μrad within 8 s. The yaw result is calculated using Eq. (3) with the calibrated equivalent length for yaw, L_{yaw} = 1.8482 mm. The yaw comparison result is shown in Figure 7 which achieves 0.48 μrad of error in standard deviation. Since pitch and yaw are adaptations of displacement measurements weighted by an equivalent length, the maximum measurement speeds (limited by Doppler shifts) for pitch and yaw angle changes are v_m/L_{pitch} and v_m/L_{yaw}, which are both approximately 12 rad/s. The linear measurement range for pitch and yaw is around 100 μrad as estimated in Ref. 27.

In the straightness comparison experiment, the stage moves back and forth along the x-axis through a range of 27 μm within 10 s. The Renishaw displacement interferometer is placed at an orthogonal measurement orientation which records the displacement along the X-axis for comparison. In our sensor, the output voltage change will be proportional to the beam centroid position change incident on the PSD sampled at 500 Hz to the host computer and the straightness errors can be calculated using Eqs. (4) and (5). Our PSD is from On-Trak Photonics, Inc. and is accompanied with the OT301 precision position sensing amplifier. The specified

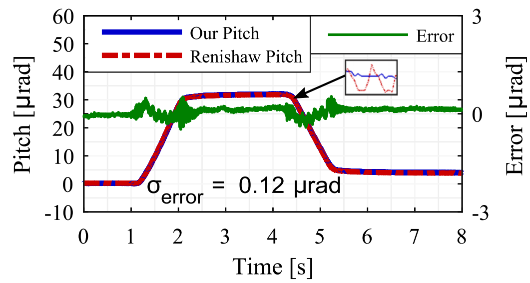

FIG. 6. The comparison result of a pitch measurement (final LPF at 30 Hz) with a Renishaw angular interferometer over 30 μrad within 8 s using a calibrated equivalent length 1.8643 mm.

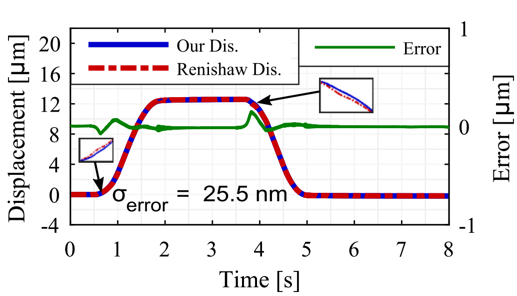

FIG. 5. The comparison result of a displacement measurement (final LPF at 30 Hz) with a Renishaw displacement interferometer over 12 μm within 8 s.

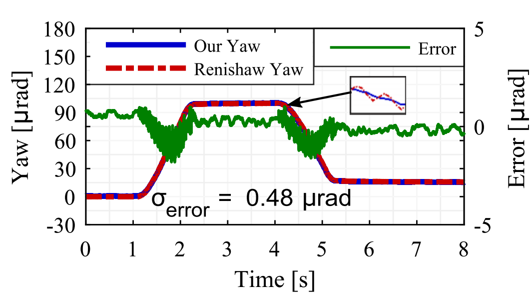

FIG. 7. The comparison result of a yaw measurement (final LPF at 30 Hz) with a Renishaw angular interferometer over 100 μrad within 8 s using a calibrated equivalent length 1.8482 mm.

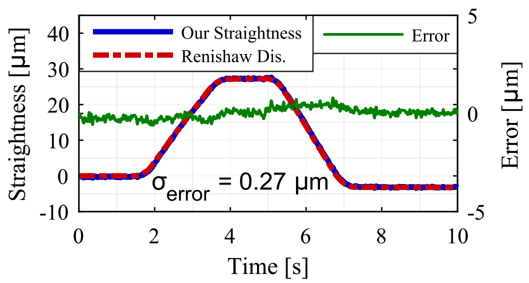

FIG. 8. The comparison result of a straightness measurement (final LPF at 70 Hz) with an orthogonally mounted Renishaw displacement interferometer over 27 μm within 10 s.

TABLE I. Repeatability of our measurement system for each DOF - representative measurements are outlined above. Measurement artifacts were not removed and re-mounted between tests.

	Test 1	Test 2	Test 3	Mean
Displacement (nm)	28.0	25.5	26.1	26.5
Pitch (μrad)	0.12	0.16	0.15	0.14
Yaw (μrad)	0.46	0.49	0.37	0.44
Straightness (μm)	0.27	0.38	0.30	0.33
Roll (μrad)	49.9	41.0	46.4	45.8

resolution of this model is on the order of 0.25 μm. Figure 8 shows a straightness comparison result along the X-axis which achieves a standard deviation error of 0.27 μm. We are unable to do the straightness comparison experiment along Y-axis because the stage cannot move along that direction. However, the working principle and performance of straightness Δy measurement will be the same as straightness Δx. Based on the beam diameter (3.3 mm) and PSD dimensions (25 mm $\times$ 25 mm), the measurement range is 10 mm.

In the roll comparison experiment, the stage rotates back and forth around the Z-axis through a range of 2.1 mrad within 25 s. A lock-in amplifier (Model SR830—Stanford Research Systems) is used to record the amplitude change of the interference signal incident on PD_2, and the PD_1 signal is set as the reference input. The sampling rate for the amplitude readout of the measurement signal is 500 Hz. The roll result is calculated using Eq. (12) and the sensitivity factor used is $k = 2.322 \times 10^{-3}$. The roll comparison result is shown in Figure 9 which can achieve 46.4 μrad in error standard deviation. Our result is compared to an orthogonal pitch measurement because the commercial system does not have the capability to measure roll directly. The approximate linear measurement range in our roll simulation shown in Figure 3 is around 35 mrad.

To examine the repeatability of our six-DOF measurement system, three consecutive tests for each DOF are conducted in the above measurement scenarios. Table I shows the standard deviation of the error compared with the Renishaw interferometer over three consecutive trials without touching the measurement artifacts between tests. It is evident that our discussed measurement system has a high level of repeatability in each DOF and achieves mean values of 26.5 nm in displacement, 0.33 μm in straightness, 0.14 μrad in pitch, 0.44 μrad in yaw, and 45.8 μrad in roll. Figure 10 shows the noise floor measurements for each DOF of our measurement system. The dominant error source for displacement, pitch, and yaw measurements will be refractive index fluctuations; it will also affect roll measurements but only based on the path difference after reference and measurement interference occurrence. Since the straightness measurement is based on a D.C. signal, it will be mainly affected by amplitude spikes, drift of electronics, and ambient lighting effects.

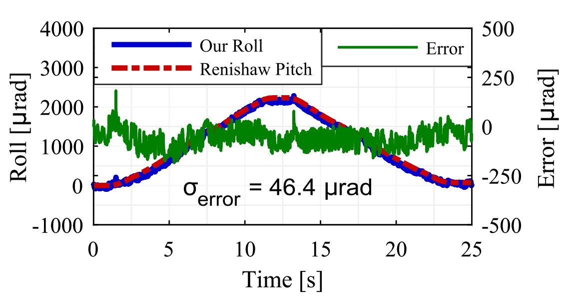

FIG. 9. The comparison result of a roll measurement (final LPF at 53 Hz) with the Renishaw angular interferometer over 2100 μrad within 25 s.

IV. CROSSTALK COMPENSATION

All measurement DOFs are independent with respect to each other except straightness and roll. Straightness accuracy is coupled to pitch and yaw because the lateral beam offset changes as a function of optical window rotation (through the semi-reflective mirror and half-wave plate in our target). Roll accuracy is coupled to pitch and yaw rotations because the HWP retardance changes as a function of those rotations. Furthermore, since the roll measurement is based on an interferometric technique, straightness errors are coupled which will modulate the signal interference amplitude due to beam walk. Lastly, to exacerbate these effects, the retro-reflector will

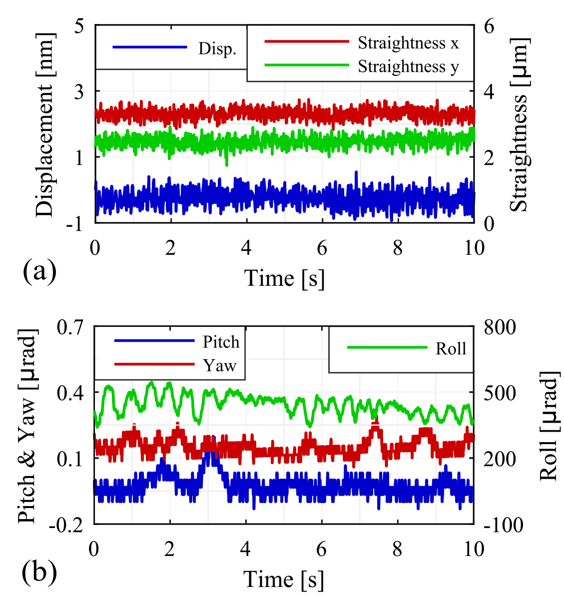

FIG. 10. The noise floors for (a) displacement and two straightness directions, (b) pitch, yaw, and roll over 10 s for our six-DOF measurement system. Data have been offset for clarity.

change the polarization state of our signal in response to roll, pitch, and yaw; however, this can be minimized by using a coated retroreflector. All of these parasitic motions are coupled into the roll measurement result and need individual compensation to achieve reliable results. In this section, we propose a compensation method that uses the other DOF measurements as feedback sensors.

A. Straightness measurement compensation

The beam will exhibit a transverse offset relative to the propagation direction after it passes through a tilted optical window, in our case, the semi-reflective mirror and half-wave plate. The lateral offset, s, can be calculated as

$$s = d\theta(1 - \frac{1}{n}), \tag{13}$$

when the optical window has a small rotation. In Equation (13), d is the width of optical window, θ (small angle) is the tilt angle, and n is the refractive index. In our setup, the refractive indices and widths for our semi-reflective mirror (crystal quartz) and half-wave plate (fused silica) are similar. Thus, the total pseudo-straightness effects in the x and y directions due to yaw and pitch can be calculated as

$$s_x = 2d\theta_y(1 - \frac{1}{n}), \tag{14}$$

$$s_y = 2d\theta_x(1 - \frac{1}{n}). \tag{15}$$

And the actual straightness measurement can be calculated as

$$\Delta x = \Delta x_{measure} - s_x, \tag{16}$$

$$\Delta y = \Delta y_{measure} - s_y, \tag{17}$$

where $\Delta x_{measure}$ and $\Delta y_{measure}$ are the direct readouts from the straightness results, and s_x and s_y are the straightness compensation terms.

B. Roll measurement compensation

To investigate how a pitch movement affects roll measurement results, we only rotate the stage around the X-axis and record the roll measurement. Figure 11 shows the measured roll result when the target only has a pitch rotation from 0 to 1800 μrad. The two parameters are mostly linear with respect to each other so we can use a linear function to represent the relationship. The standard deviation of error represented by this linear fitting function $y = 0.3126x - 2.4641$ is 10.7 μrad. The relationship between a roll readout caused by yaw rotation is shown in Figure 12 and the linear fitting function is $y = 0.3898x - 23.1481$, which leads to 16.7 μrad in standard deviation of the error.

The retroreflector's straightness errors will cause the f_2 beam center to move, which reduces the interference signal in PD_2. To investigate the straightness parasitic influence, we only move the stage along the X-axis and record the roll measurement. Figure 13 shows the measured roll result when the target performs a straightness movement from 0 to 45 μm. The relationship is not perfectly linear, but the general trend can still be represented by a linear fitting function $y = 17.1065x - 19.0094$, which leads to 39.1 μrad in standard deviation of the error.

Thus, the pseudo roll readout caused by parasitic motions is the combination of the above situations, which can be expressed as

$$\Delta\theta_z = 0.3126\theta_x + 0.3898\theta_y - 17.1065\sqrt{(\Delta x)^2 + (\Delta y)^2} - 6.6028. \tag{18}$$

In practice, the measured roll result can be compensated by an equation of this form and the actual roll measurement result can be calculated by

$$\theta_z = \theta_{z,measure} - \Delta\theta_z, \tag{19}$$

where $\theta_{z,measure}$ is the direct readout of the roll result and $\Delta\theta_z$ is the roll compensation term. It should be noted that the linear scaling of the yaw crosstalk compensation might change as a function of pitch and *vice versa*. The full, potentially coupled crosstalk compensation is left as a subject of future work in addition to a more complete treatment of the performance of this instrument.

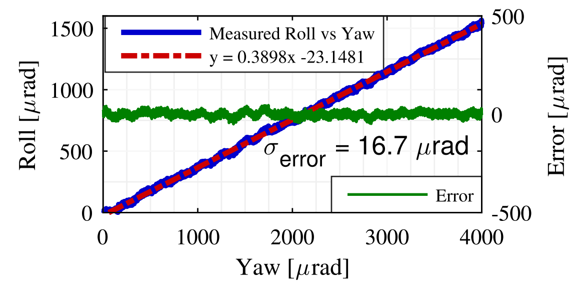

FIG. 12. The roll readout caused by a yaw motion within 4000 μrad and its linear fitting function.

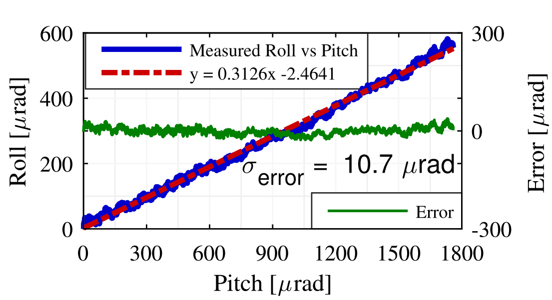

FIG. 11. The roll readout caused by a pitch motion within 1800 μrad and its linear fitting function.

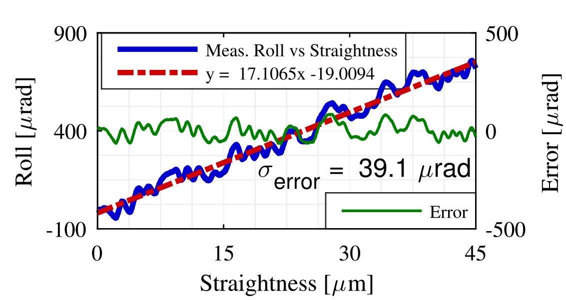

FIG. 13. The roll readout caused by straightness motion within 45 μm and its linear fitting function.

V. CONCLUSION

A compact, fiber-coupled, six-DOF measurement system which enables fast, accurate calibration, and error mapping of a precision linear stage is presented. The novel system can simultaneously measure six-DOF geometric errors using a single optical beam traveling between the measurement system and a small target. The comparison experiments with a commercial interferometer for each DOF measurement demonstrate that our system can achieve high resolution and accuracy.

The working principle for longitudinal z-displacement measurements is a typical heterodyne displacement interferometer, with a measurement range on the order of meters. Although pitch and yaw measurements operate with the same interferometric principles, the linear range is limited to nominally 100 μrad as estimated in the previous work.[27] Straightness measurement range is based on a combination of beam diameter and PSD active area. Based on our experimental beam diameter (3.3 mm) and PSD dimensions (25 mm $\times$ 25 mm), the straightness range is 10 mm. Finally, roll measurement range is driven by the linearity of the simulation shown in Figure 3. Based on the linear portion of that figure, roll can be measured within a 35 mrad range.

The influences of crosstalk effects on roll and straightness measurements are discussed in detail and compensation methods are proposed. Utilizing the discussed system will enable calibration and error mapping of multiple axes simultaneously, largely simplifying and shortening the calibration period while minimizing calibration errors.

ACKNOWLEDGMENTS

The authors would like to thank Chen Wang from the University of Rochester and Dr. Stephen C. Howard of InSituTec Incorporated for the fruitful discussions regarding this work. The authors would like to acknowledge the support of the US Department of Commerce, National Institute of Standards and Technology under Award No. 70NANB12H186 and Award No. 70NANB14H266, and the National Science Foundation under Award Nos. CMMI:1265824 and IIP:1417032.

[1]N. Bobroff, Meas. Sci. Technol. **4**, 907 (1993).
[2]H. Bosse and G. Wilkening, Meas. Sci. Technol. **16**, 2155 (2005).
[3]C.-m. Wu, J. Lawall, and R. D. Deslattes, Appl. Opt. **38**, 4089 (1999).
[4]J. Lawall and E. Kessler, Rev. Sci. Instrum. **71**, 2669 (2000).
[5]K.-N. Joo, J. D. Ellis, E. S. Buice, J. W. Spronck, and R. H. M. Schmidt, Opt. Express **18**, 1159 (2010).
[6]J. D. Ellis, A. J. Meskers, J. W. Spronck, and R. H. M. Schmidt, Opt. Lett. **36**, 3584 (2011).
[7]Z. Ge and M. Takeda, Appl. Opt. **42**, 6859 (2003).
[8]M.-H. Chiu, S.-F. Wang, and R.-S. Chang, Appl. Opt. **43**, 5438 (2004).
[9]S. Chatterjee and Y. P. Kumar, Appl. Opt. **47**, 4900 (2008).
[10]I. Hahn, M. Weilert, X. Wang, and R. Goullioud, Rev. Sci. Instrum. **81**, 045103 (2010).
[11]K.-C. Fan, C.-L. Chu, J.-L. Liao, and J.-I. Mou, Meas. Sci. Technol. **14**, 47 (2003).
[12]Q. Feng, B. Zhang, and C. Kuang, Opt. Laser Technol. **36**, 279 (2004).
[13]C.-m. Wu, Appl. Opt. **43**, 3812 (2004).
[14]C. Kuang, E. Hong, Q. Feng, B. Zhang, and Z. Zhang, Meas. Sci. Technol. **18**, 3795 (2007).
[15]S. Li, C. Yang, E. Zhang, and G. Jin, Opt. Lett. **30**, 242 (2005).
[16]Y. Le, W. Hou, K. Hu, and K. Shi, Opt. Lett. **38**, 3600 (2013).
[17]S. R. Gillmer, X. Yu, C. Wang, and J. D. Ellis, Opt. Lett. **40**, 2497 (2015).
[18]C.-H. Liu, W.-Y. Jywe, C.-C. Hsu, and T.-H. Hsu, Rev. Sci. Instrum. **76**, 055110 (2005).
[19]X. Li, W. Gao, H. Muto, Y. Shimizu, S. Ito, and S. Dian, Precis. Eng. **37**, 771 (2013).
[20]F. Qibo, Z. Bin, C. Cunxing, K. Cuifang, Z. Yusheng, and Y. Fenglin, Opt. Express **21**, 25805 (2013).
[21]H.-L. Hsieh and S.-W. Pan, Opt. Express **23**, 2451 (2015).
[22]B. Chen, B. Xu, L. Yan, E. Zhang, and Y. Liu, Opt. Express **23**, 9052 (2015).
[23]T. Schuldt, M. Gohlke, D. Weise, U. Johann, A. Peters, and C. Braxmaier, Classical Quantum Gravity **26**, 085008 (2009).
[24]G. Hechenblaikner, J. Opt. Soc. Am. A **27**, 2078 (2010).
[25]G. Wanner, G. Heinzel, E. Kochkina, C. Mahrdt, B. S. Sheard, S. Schuster, and K. Danzmann, Opt. Commun. **285**, 4831 (2012).
[26]S. R. Gillmer, R. C. G. Smith, S. C. Woody, and J. D. Ellis, Meas. Sci. Technol. **25**, 075205 (2014).
[27]X. Yu, S. Gillmer, and J. Ellis, Meas. Sci. Technol. **26**, 125203 (2015).